Transport characteristics of DNA-tagged silica colloids as a colloidal tracer in saturated sand columns; role of solution chemistry, flow velocity, and sand grain size

Kianfar, Bahareh; Tian, Jingya; Rozemeijer, Joachim; van der Zaan, Bas; Bogaard, Thom A.; Foppen, Jan Willem

DOI
10.1016/j.jconhyd.2022.103954

Publication date
2022

Document Version
Final published version

Published in
Journal of Contaminant Hydrology

Journal of Contaminant Hydrology 246 (2022) 103954

Contents lists available at ScienceDirect

Journal of Contaminant Hydrology

journal homepage: www.elsevier.com/locate/jconhyd

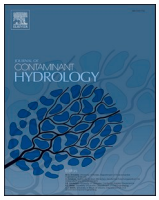

Transport characteristics of DNA-tagged silica colloids as a colloidal tracer in saturated sand columns; role of solution chemistry, flow velocity, and sand grain size

Bahareh Kianfar [a,*], Jingya Tian [b], Joachim Rozemeijer [c], Bas van der Zaan [c], Thom A. Bogaard [a], Jan Willem Foppen [a,b,**]

[a] Department of Water Management, Faculty of Civil Engineering and Geosciences, Delft University of Technology, Delft, the Netherlands
[b] Department of Water Resources and Ecosystems, IHE-Delft Institute for Water Education, Delft, the Netherlands
[c] Deltares, Utrecht, the Netherlands

ARTICLE INFO

Keywords:
DNA-tagged silica colloids
Tracer
Solution chemistry

ABSTRACT

In recent years, DNA-tagged silica colloids have been used as an environmental tracer. A major advantage of this technique is that the DNA-coding provides an unlimited number of unique tracers without a background concentration. However, little is known about the effects of physio-chemical subsurface properties on the transport behavior of DNA-tagged silica tracers. We are the first to explore the deposition kinetics of this new DNA-tagged silica tracer for different pore water chemistries, flow rates, and sand grain size distributions in a series of saturated sand column experiments in order to predict environmental conditions for which the DNA-tagged silica tracer can best be employed. Our results indicated that the transport of DNA-tagged silica tracer can be well described by first order kinetic attachment and detachment. Because of massive re-entrainment under transient chemistry conditions, we inferred that attachment was primarily in the secondary energy minimum. Based on calculated sticking efficiencies of the DNA-tagged silica tracer to the sand grains, we concluded that a large fraction of the DNA-tagged silica tracer colliding with the sand grain surface did also stick to that surface, when the ionic strength of the system was higher. The experimental results revealed the sensitivity of DNA-tagged silica tracer to both physical and chemical factors. This reduces its applicability as a conservative hydrological tracer for studying subsurface flow paths. Based on our experiments, the DNA-tagged silica tracer is best applicable for studying flow routes and travel times in coarse grained aquifers, with a relatively high flow rate. DNA-tagged silica tracers may also be applied for simulating the transport of engineered or biological colloidal pollution, such as microplastics and pathogens.

1. Introduction

Tracers are widely used in hydrological studies, such as tracking contamination in the subsurface.

In recent years, DNA-tagged silica colloids (abbreviated to DNAcol) have been used as an environmental tracer in various applications, e.g., in fractured reservoir characterization (Zhang et al., 2015), in a coarse-grained aquifer (Mikutis et al., 2018), in fractured crystalline rock (Kittilä et al., 2019), and at smaller scale for tomographic reservoir imaging (Kong et al., 2018). The use of silica colloids tagged with DNA is not limited to water and oil applications: examples include pesticide spraying (Mora et al., 2015), and waste water sludge (Grass et al., 2014). More recently, DNAcol were also used as a surrogate model to study the microbial transmission in healthcare (Scotoni et al., 2020), and in the setting up of a "DNA-of-things" as the storage material (Koch et al., 2020). The main advantages of tagging silica colloids with DNA are that it gives the colloids a unique DNA sequence and enables analysis at low concentrations using standard microbial techniques (e.g. quantitative polymerase chain reaction (qPCR)). These properties provide us with a virtually unlimited amount of unique tracer particles which make

* Corresponding author.
** Corresponding author at: Department of Water Management, Faculty of Civil Engineering and Geosciences, Delft University of Technology, Delft, the Netherlands.
E-mail addresses: b.kianfar@tudelft.nl (B. Kianfar), j.foppen@un-ihe.org, J.W.A.Foppen@tudelft.nl (J.W. Foppen).

https://doi.org/10.1016/j.jconhyd.2022.103954
Received 7 June 2021; Received in revised form 23 December 2021; Accepted 1 January 2022
Available online 17 January 2022

DNAcol a promising tool for hydrological and colloidal contaminant transport research.

Transport of colloids through saturated porous media is often described at the continuum scale (i.e., macroscopic scale) with the classic advection–dispersion partial differential equation (e.g. Elimelech et al., 1995; Ryan and Elimelech, 1996; Molnar et al., 2015; Molnar et al., 2019), using a first-order kinetic retention parameter. This parameter can be correlated to colloid filtration theory using a mechanistical model, including the use of a correlation equation (e.g. Yao et al., 1971; Ma et al., 2013; Long and Hilpert, 2009; Rajagopalan and Tien, 1976; Tufenkji and Elimelech, 2004; Nelson and Ginn, 2011), to estimate the trajectory of a colloid near a collector. More recently, the importance of colloid size dependent dispersion (Chrysikopoulos and Katzourakis, 2015), gravity effects of colloids (Chrysikopoulos and Syngouna, 2014), mechanical equilibrium and maximum retention function (Bedrikovetsky et al., 2011; Bedrikovetsky et al., 2012), fraction of the collector surface area (S_f) contributing to colloid attachment, and importance of applied hydrodynamic and adhesive torques (Bradford et al., 2009; Bradford et al., 2015), concentration dependent colloid transport (Bradford et al., 2009), and nanoscale heterogeneity (Bradford et al., 2015; Ron et al., 2019; Ron and Johnson, 2020) were explored and highlighted.

When silica colloids travel in columns of saturated quartz sand, their transport can be characterized by first order kinetic attachment to the sand (Liu et al., 2017; Kim et al., 2015; Wang et al., 2012; Zeng et al., 2017; Saiers et al., 1994; Johnson et al., 1996; Vitorge et al., 2014, 2014a), which is more or less depending on ionic strength (Liu et al., 2019; Zeng et al., 2017; Kim et al., 2015), pH (Liu et al., 2019), pore water flow velocity (Kim et al., 2015, their exp. 5 and 9), composition of the collector surface (Johnson et al., 1996; Ryan et al., 1999; Ko and Chen, 2000; Li and Cathles, 2014; Liu et al., 2017) or presence of humics (Zhou et al., 2017; Zhang et al., 2020). Furthermore, size exclusion effects might play a role (e.g. Fig. 10a of Higgo et al., 1993; Mikutis et al., 2018). Finally, silica colloids can enhance contaminant transport (Dai et al., 2020; Hou et al., 2021; Mendes de Oliveira et al., 2017; Qin et al., 2020). In the subsurface, therefore, all of the aforementioned physicochemical factors can influence aggregation, deposition, and remobilization of colloidal matter. To better predict the behavior of DNAcol as a tracer or surrogate we conducted a series of saturated sand column experiments.

The objective of this study was two-fold. First, to systematically explore the use of DNAcol in columns of quartz sand in order to compare deposition kinetics with existing literature. Second, we wanted to identify removal of DNAcol under various saturated porous media conditions in order to start predicting their value in environmental applications. Thereto, we carried out column experiments with DNAcol in which we varied solution chemistry, flow rate and grain size. In addition, we used HYDRUS-1D to quantify transport parameters and assist in analyzing colloid-grain surface interaction processes.

2. Materials and methods

2.1. The DNA-tagged silica particle

The DNAcol was composed of a silica outer shell (SiO_2), a layer of DNA molecules, and a silica core (Paunescu et al., 2013). A 1 ml 10 mg ml^{-1} DNAcol suspension, equal to ~4×10^{11} particles ml^{-1} (Paunescu et al., 2013), was kindly fabricated and provided by the Functional Materials Laboratory Group at ETH Zurich. Average diameter of DNA-tagged silica particles was ~270 nm, and density of 2.2 g cm^{-1} (Mora et al., 2015).

The double-stranded DNA sequence, which was sandwiched between silica core and protective cover layer, was 80 nucleotides long (details in the Supporting Information). Prior to use, DNAcol was washed in a diluted commercial bleach solution (10 μl bleach to 10 ml water) to ensure no free DNA in suspension. Then, 1000× diluted DNAcol batches (5 μl to 5 ml; DNAcol concentration = 0.001 mg ml^{-1} or ~ 4×10^7 particles ml^{-1}) were prepared in Milli-Q water, NaCl (33 mM, pH = 5.5), and $CaCl_2$ (41 mM, pH = 5.8).

The effect of solution chemistries on the stability of DNAcol was measured via the zeta potential (ζ) using a NanoSizer (Nano Series, Malvern Instrument Ltd., UK). The ζ was determined from electrophoretic mobility using Smoluchowski's formula (at 25 °C temperature, and the dielectric constant of water medium 78.54). Thereto, three DNAcol batches were prepared in Milli-Q water (resistivity 18 MΩ cm), NaCl (IS = 33 mM, pH = 5.5), and $CaCl_2$ (IS = 41 mM, pH = 5.8) in a 10 ppm concentration (0.01 mg ml^{-1}). After vortexing, ζ was −42.5 ± 5.3 mV in Milli-Q water, −33.9 ± 6.1 mV in NaCl, and − 20.7 ± 3.3 mV in $CaCl_2$ solution, respectively. We used these values for DLVO calculations (see Supporting Information).

2.2. Porous medium

We used two different sand types. One was quartz sand (J.T. Baker, Inc., Phillipsburg, New Jersey) sieved to a fraction of 1000–1400 μm grain size range (coarse sand), and the other was so-called silver sand (M31, Sibelco, Belgium) sieved to a fraction of 500–630 μm grain size range (fine sand). To remove impurities, the sands were soaked in 65% concentrated 4 N HNO_3 solution for 2 h at 100 °C. After cooling, the acid was decanted and the sand was rinsed repeatedly with deionized water until the pH stabilized around 7 and the electrical conductivity of the rinse water became less than 1–2 μS cm^{-1}. Then the acid-washed sand was oven dried for 24 h at 105 °C. The clean and dry sand was stored in a capped container for further use. The zeta potential of both fine and coarse sand was determined with a crushed fraction. Thereto, both fine and coarse sand were ground manually using a mortar and pestle. Then, ~0.5 g of crushed sand was added to 10 ml of each Milli-Q water, NaCl, and $CaCl_2$ solution. Each suspension was vortexed three times and allowed to settle for 2 min. The supernatant was used for measuring the zeta potential. The ξ for fine sand was −34.4 ± 5.4 mV (in Milli-Q water), −39.4 ± 5.4 mV (in NaCl), and − 15.3 ± 4.3 mV (in $CaCl_2$) while for coarse sand it was −33.1 ± 4.7 mV (in Milli-Q water), −41.2 ± 7.1 mV (in NaCl), and − 11.3 ± 4.5 mV (in $CaCl_2$). The mean and standard deviation values are calculated from the average of mean and standard deviation of triplicate measurements.

2.3. Column experiments

Soil column experiments were conducted with adjustable-height chromatography columns, made of borosilicate glass (Omnifit, Cambridge, UK). The column, with an inner diameter of 2.5 cm, was wet-packed with one of the two sands to a height of 6.5 cm. Before packing the column, CO_2 gas was flushed into the dry sand to increase wettability of the sand upon wet-packing. During wet-packing, the column was vibrated with a plastic bar to facilitate uniform packing. After connecting the pump, demineralized water was injected in an upward direction at a constant flow rate. Typically, two columns were prepared; one with fine sand, and one with coarse sand. These columns were run in parallel at similar pump speed (see Table 1 for an overview). First, 2–2.5 pore volumes of NaCl solution was injected in order to determine dispersivity and porosity of the sand. Thereto, at specific time intervals, as a proxy for NaCl-concentration, the Electrical Conductivity (EC) of the effluent was measured. Then, the influent solution was switched back to Demineralized water (DM water) to flush out remaining NaCl solution. Next, a 2–2.5 Pore Volumes (PV) of a 10^{-3} mg ml^{-1} (~ 4×10^7 particles ml^{-1}) DNAcol suspension in DM water under continuous mixing was injected in the column, followed by at least 3 PV flushing with DNAcol-free solution. The column was flushed overnight with NaCl, and then a 2–2.5 PV of a 10^{-3} mg ml^{-1} (~ 4×10^7 particles ml^{-1}) DNAcol suspension in NaCl under continuous mixing was injected in the column, followed by at least 3 PV flushing with DNAcol-free solution. The column was flushed overnight with $CaCl_2$, and then a 2–2.5 PV of a 10^{-3}

Table 1
Overview of experimental conditions for column experiments with DNAcol.

Solution chemistry[1]	Sand[2]	Flow[3]	Data shown in fig1	Remarks
DM water	Coarse	High	1E	
	Fine	High	1F	
	Coarse	Low	1G	
	Fine	Low	1H	
NaCl	Coarse	High	1I	
	Fine	High	1J	
	Coarse	Low	1K	Extra Milli-Q water flush
	Fine	Low	1L	Extra Milli-Q water flush
$CaCl_2$	Coarse	High	1M	
	Fine	High	1N	
	Coarse	Low	1O	Extra Milli-Q water flush
	Fine	Low	1P	Extra Milli-Q water flush

[1] DM: demineralised water; [NaCl] = 33 mM (pH = 5.5); [$CaCl_2$] = 41 mM (pH = 5.8).
[2] Coarse sand: 1000–1400 μm; fine sand: 500–630 μm.
[3] High flow: pump rate 0.8 ± 0.02 ml min^{-1}; low flow: pump rate 0.16 ± 0.01 ml min^{-1}.

mg ml^{-1} (~ 4×10^7 particles ml^{-1}) DNAcol suspension in $CaCl_2$ under continuous mixing was injected in the column, followed by at least 3 PV flushing with DNAcol-free solution. So, per column, a total of 4 experiments were carried out. The tubing pore volume was negligible.

For a number of experiments ('Extra Milli-Q water flush' in see Table 1) at the end of the experiment we applied a 3 PV flush of demineralized water in order to mimic transient chemistry conditions and to possibly re-entrain previously attached DNAcol. Most experiments were carried out in duplicate. For each experiment ~0.8 ml column effluent was collected in a 20-ml centrifuge tube using a fraction collector (OMNICOLL, LAMBDA Laboratory Systems, Switzerland). Of this, 100 μl was pipetted into a 1.5 ml Eppendorf vial and stored at 4 °C in the fridge for DNA release and qPCR analysis later.

2.4. DNA release and qPCR analysis

The concentration of DNA in a sample was determined using the qPCR technique. In order to dissolve the silica shell and release the encapsulated DNA, 20 μl of collected sample was mixed with 1 μl of buffer oxide etch (BOE; a mixture of NH_4FHF (Merck, Germany) and NH_4F (Sigma-Aldrich), diluted 10 times in Milli-Q water; see for details Paunescu et al., 2013). After this, 100 μl Tris-HCl buffer at pH 8.3 was added to adjust pH to near-neutral value, and of this 5 μl was added to each qPCR tube (8-tube strip) (BIOplastics, the Netherlands), together with 1 μl of each forward and reverse primer (DNA oligomers (Biolegio, Nijmegen, Netherlands)): 5′-GAT TAGCTT GAC CCG CTC TG-3′ and 5′-AGT TGG GGT TTG CAG TTG TC-3′), 10 μl Kapa SYBR Green Fast qPCR Mastermix (Kapa biosystems, Sigma-Aldrich), and 3 μl DEPC treated water (Sigma-Aldrich). The pre-qPCR samples tubes were closed with optical 8-cap strip (BIOplastics, the Netherlands). Sample preparation of first set of experiments was done by manual pipetting; later, qPCR sample preparation was carried out using a pipetting robot (QIAgility instrument; Qiagen, Hilden, Germany). DNA concentrations were determined using a Mini-Opticon (Bio-Rad, Hercules, CA, USA) programmed to run 400 s at 95 °C and then 42 cycles of [14 s at 95 °C, 27 s at 58 °C, 25 s at 72 °C]. Results in terms of threshold cycles (Ct) were analyzed using the Bio-Rad CFX Manager 3.1 software and applying the regression function in the Cq determination mode (as opposed to the manually adjustable baseline subtraction). DNAcol concentrations were then read from a calibration curve from duplicated samples, which was prepared for each solution chemistry (Supporting Information).

2.5. Modeling transport of DNAcol

Transport of silica colloids in saturated porous media can be described by the advection-dispersion equation with first order attachment and detachment (e.g. Saiers et al., 1994; Kim et al., 2015; Zhou et al., 2017; Zeng et al., 2017):

$$\frac{\partial C}{\partial t}+\frac{\rho_b}{\theta}\frac{\partial S}{\partial t}=\lambda_L v\frac{\partial^2 C}{\partial x^2}-v\frac{\partial C}{\partial x} \quad (1)$$

$$\rho_b\frac{\partial S}{\partial t}=k_{att}\theta C-k_{det}\rho_b S \quad (2)$$

where C is the concentration of silica colloid in the aqueous phase [ML^{-3}], S is the concentration of silica colloid in the solid phase [MM^{-1}], ρ_b is the dry bulk density [ML^{-3}], θ is volumetric water content [M^3M^{-3}], t is time [T], λ_L is the dispersivity [L], ν is the pore water velocity [LT^{-1}], x is the traveled distance (length) [L], and k_{att} and k_{det} are attachment and detachment rate coefficients [T^{-1}], respectively. A large number of advection-dispersion models have been developed to describe solute and colloid transport in porous media analytically and/or numerically, either with one- or two-site kinetic attachment or adsorption (Selim et al., 1987; Van Genuchten and Wagenet, 1989; Van Genuchten et al., 2012; Katzourakis and Chrysikopoulos, 2017; Schijven and Šimůnek, 2002; Katzourakis and Chrysikopoulos, 2019). In this work, we used HYDRUS-1D (Šimůnek et al., 2013) to determine values of dispersivity, porosity, and attachment and detachment rate coefficients. The first two parameters (i.e., dispersivity (λ_L), porosity (ε)) were determined by fitting the NaCl tracer data, while for the latter two parameters (first-order attachment (k_{att}), and detachment rate coefficients (k_{det})) the DNAcol breakthrough data were used by invoking porosity and dispersivity values obtained from the NaCl tracer experiment, whereby the code was set to log-resident concentrations. In doing so, we excluded colloid size dependent dispersivity and mechanical equilibrium (see Introduction section). The former assumption underestimated colloid dispersivity. Also, gravity effects were excluded, since the DNAcol was small resulting in negligible restricted settling velocity as a function of column orientation and flow direction (Chrysikopoulos and Syngouna, 2014). The model presented here (Eqs. (1) and (2)) is implemented in the HYDRUS-1D software package (Šimůnek and van Genuchten, 2008). Briefly, a Galerkin-type linear finite element method was used for spatial discretization, while finite difference methods were used to approximate temporal derivatives, and a Crank–Nicholson finite difference scheme was used for solution of the advection–dispersion equation. Parameter optimization was carried out by first defining an objective function (Šimůnek et al., 1998), which was then minimized using the Levenberg-Marquardt non-linear minimization method, which is a weighted least-squares approach based on Marquardt's maximum neighborhood method (Marquardt, 1963). We used HYDRUS-1D because it is open source, widely-used and well documented, and it includes various colloid transport models, including the one we used.

The dimensionless sticking efficiency, α, was then determined from (e.g. Wang et al., 2012; Lutterodt et al., 2021; Tufenkji and Elimelech, 2004; Harvey and Garabedian, 1991; Ryan and Elimelech, 1996):

$$\alpha=k_{att\_HYDRUS}\frac{2d_g}{3(1-\varepsilon)v\eta_0} \quad (3)$$

where k_{att_HYDRUS} is the attachment rate coefficient obtained from HYDRUS modeling, η_0 is the single collector efficiency [−], ε is porosity of sand column [−], and d_g the collector or sand grain diameter [L]. The sticking efficiency is defined as the fraction of DNAcol sticking to the sand grain surface over the total DNAcol colliding with the sand grain surface. When $\alpha = 0$, then no DNAcol would stick to the surface and when $\alpha = 1$ then all DNAcol colliding would also stick. The collision efficiency was determined using the Tufenkji and Elimelech (TE) correlation equation (Tufenkji and Elimelech, 2004). Thereto, 2.2 g cm^{-3}

was assumed for the DNAcol (Mora et al., 2015), while the Hamaker constant was assumed to be 0.7×10^{-20} J for the combination of silica-water-silica (Rhodes, 2008).

2.6. Evaluating hypothetical DNAcol removal upon traveled distance

When the flow field is in steady state, and when transport of DNAcol is considered to be one-dimensional and in steady state without detachment, then the mass balance for DNAcol in the fluid phase reduces to:

With boundary conditions

$$\lambda_L v \frac{d^2C}{dx^2} - v\frac{dC}{dx} - k_{att}C = 0 \tag{4}$$

$$C(0) = C_0 \; and \; \frac{dC}{dx}(\infty) = 0 \tag{5}$$

Eq. (4) can be solved analytically (Van Genuchten, 1981):

$$C = C_0 exp\left\{\frac{\left(v - v\left(\frac{4k_{att}\lambda_L v}{v^2}\right)^{\frac{1}{2}}\right)x}{2\lambda_L v}\right\} \tag{6}$$

whereby

$$k_{att} = \frac{3(1-\varepsilon)}{2d_g}v\eta_0\alpha \tag{7}$$

For sticking efficiency values obtained from our experiments, a series of hypothetical collector grain sizes, and a representative Darcy groundwater flow velocity, we used Eqs. (6) and (7) to predict DNAcol removal as a function of transport distance and to evaluate the usefulness of DNAcol in aquifer experiments at three different distances.

3. Results

3.1. Column breakthrough curves (BTCs)

In case of NaCl, from 0 to 0.5 PV, the relative concentration $(C/C_0)_{NaCl}$, whereby C is the effluent EC-value as a proxy for NaCl concentration and C_0 the influent EC-value, was around 1×10^{-3} (see Fig. 1A-D). The values were not lower, since the EC of the sand column effluent prior to NaCl injection was around 1–2 μS cm^{-1}, and the EC of the NaCl tracer injected through the column was around 4×10^3 μS cm^{-1}. At PV = 1, $(C/C_0)_{NaCl}$ in all cases reached 0.5 and then continued to rise to 1. At PV 2–2.5 when $(C/C_0)_{NaCl}$ was ~1, we stopped injection of NaCl tracer. We considered this to be of sufficient contrast to determine dispersivity and porosity with HYDRUS-1D. The shape of the NaCl tracer breakthrough curve also confirmed the setup of the column in all cases was adequate, without leakage, and the front displacement inside the column was perpendicular to flow. In our experimental conditions, since Peclet numbers were high (>> 1; an indication of advection-

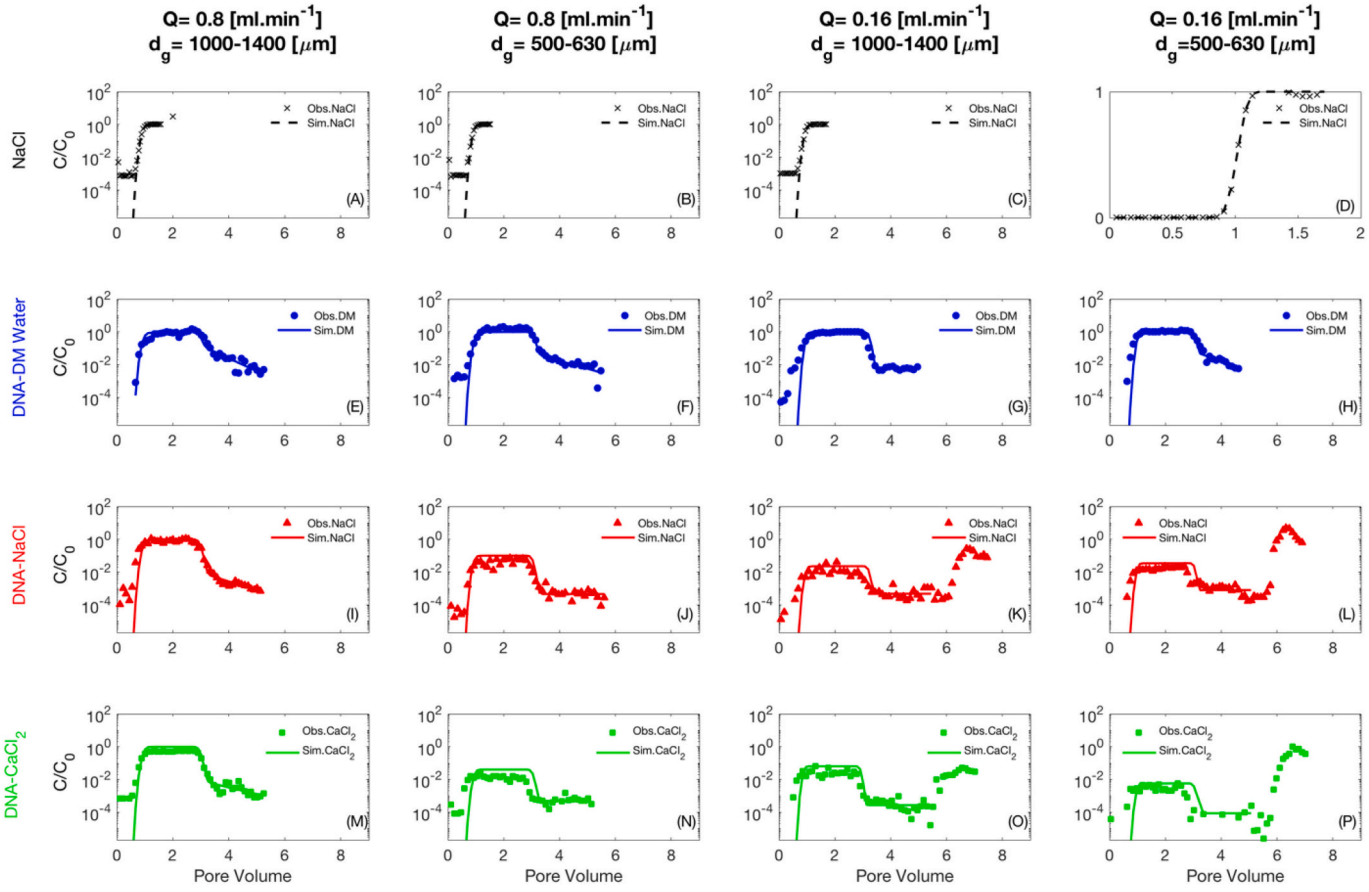

Fig. 1. Experimental data of NaCl tracer, DNAcol (symbols) and fitted breakthrough curves with HYDRUS (lines). Different panels illustrate relative concentrations as a function of pore volume within the sand columns at two different pump rates (0.8 ml $min^{-1}$and 0.16 ml min^{-1}), two types of sand (d_g = 1000–1400 μm (coarse sand) and 500–630 μm (fine sand)), and three solution chemistries (DM water, NaCl, $CaCl_2$). First row: NaCl tracer; second row: DNAcol breakthrough curves in DM water; third row: DNAcol breakthrough curves in NaCl; final row: DNAcol breakthrough curves in $CaCl_2$; first column: coarse sand-fast flow, second column: fine sand-fast flow, third column: coarse sand-low flow, final column: fine sand-low flow. Note, panel (D) is in a linear scale.

dominant transport), the dispersivity value of DNAcol was taken from the NaCl tracer experiments.

Upon injection of DNAcol in DM water, $(C/C_0)_{DNAcol}$ started to rise slightly difference than the initial rise of the NaCl tracer (Fig. 1E-H). At 1.5–2.0 PV $(C/C_0)_{DNAcol}$ reached ~1 (Fig. 1E-H). During elution, $(C/C_0)_{DNAcol}$ rapidly decreased at PV 3–4, and at PV 4–6, the tail of the breakthrough curve in most cases flattened (Fig. 1E-H).

In case of DNAcol in NaCl more specifically the coarse sand - high flow case (Fig. 1I), the moment of rise, rising limb, plateau phase, and declining limb of $(C/C_0)_{DNAcol}$ were comparable to $(C/C_0)_{DNAcol}$ in DM water. In other words, attachment was negligible in this case. However, for the fine sand and/or low flow rates conditions, maximum $(C/C_0)_{DNAcol}$ during the plateau phase decreased from ~0.06 in Fig. 1J to ~0.02 in case of Fig. 1K and L. During elution (after PV 3.5), $(C/C_0)_{DNAcol}$ in NaCl declined sharply, and, after PV 4, became constant at $\sim 1 \times 10^{-3}$ (Fig. 1K-L). In case of Fig. 1K and L, an extra Milli-Q water flush was passed through the columns, giving rise to a peak $(C/C_0)_{DNAcol}$ at ~ PV 7 of ~200 times the maximum $(C/C_0)_{DNAcol}$ during the plateau phase in Fig. 1L.

In case of DNAcol in $CaCl_2$ (Fig. 1M-P), maximum $(C/C_0)_{DNAcol}$ during the plateau phase was 0.5 (Fig. 1M), and this value decreased to 0.015 for Fig. 1N and O, and to ~0.004 for Fig. 1P, respectively. After ~ PV 4, during elution, $(C/C_0)_{DNAcol}$ of Fig. 1M remained rather high at $\sim 1 \times 10^{3}$, while for the other BTCs (Fig. 1N-P), $(C/C_0)_{DNAcol}$ during tailing was lower at $\sim 1 \times 10^{-4}$ to 1×10^{-3}. Like in the NaCl case, an extra Milli-Q water flush, which was passed through the columns (Fig. 1O and P), gave rise to a peak $(C/C_0)_{DNAcol}$ at ~ PV 7 of ~200 times the maximum $(C/C_0)_{DNAcol}$ during the plateau phase (Fig. 1P).

Finally, in some BTCs (e.g. Fig. 1I and J), from 0 to 0.5 PV the $(C/C_0)_{DNAcol}$ varied between 1×10^{-4} and 1×10^{-3}. This was because we used SYBR Green to detect DNA. SYBR-Green is a non-specific dye, which also shows amplification of non-target DNA. In fact, when $(C/C_0)_{DNAcol}$ was $\sim 1 \times 10^{-4}$ the detection limit of the qPCR analysis was reached. See Supporting Information for details regarding the standard curves, negative control, or no-template control (NTC), the lowest limit of detection level. The cutoff value was assigned to Ct = 30.

3.2. Modeling with HYDRUS and determining sticking efficiencies

All DNAcol BTCs could be well fitted with an attachment rate (k_{att}) and a detachment rate coefficient (k_{det}): except for the experiment in $CaCl_2$ fine sand-low flow yielding very low breakthrough, the R^2 values of the models ranged between 25 and 92% (Table 2). Fitted curves overestimated $(C/C_0)_{DNAcol}$ between PV 2 and 3, which gave rise to somewhat lowered R^2-values. Attachment of DNAcol in DM water was lowest with k_{att} ranging from 2.68×10^{-4} to 9.37×10^{-3}, while in $CaCl_2$ k_{att} of DNAcol was highest and ranged from 5.78×10^{-3} to 1.97×10^{-1}. For detachment, we observed the opposite: in DM water, k_{det} ranged from 2.32×10^{-3} to 1.07×10^{-1} and was relatively high, while in $CaCl_2$, k_{det} ranged from 8.56×10^{-6} to 5.25×10^{-2}, which was, relatively speaking, the lowest set of detachment rate coefficients. We identified three reasons for the 25–92% efficiency variations. Firstly, the high sensitivity of the qPCR technique, which is essentially an enzyme-based technique to determine concentrations, we used in detecting target DNA in each sample. A variation/error of Cq values was inevitable, because errors may propagate from pipetting or intrinsic variances of enzymatic efficiency due to minor temperature differences in the qPCR apparatus (Foppen et al., 2013). Secondly, the use of the one-site kinetic model (Eqs. (1) and (2)) may have oversimplified the true DNAcol transport processes in the columns. Thirdly, we observed that the model could not capture the earlier breakthrough curve of DNAcol data in several cases. This limitation was associated with assigning the dispersivity value of NaCl tracer to the DNAcol. As mentioned in the Methods Section, such assumption can lead to underestimation of the colloid dispersivity.

From k_{att} values determined with HYDRUS, we calculated the sticking efficiency values of the DNAcol per experiment by making use of Eq. (3) (Table 2). In DM water, sticking efficiencies ranged from 0.008–0.27 and in both NaCl and $CaCl_2$, sticking efficiencies ranged from ~0.02 to 1.56. Based on these values we concluded that sticking efficiencies in DM water were relatively lowest, while in NaCl and $CaCl_2$ they were highest. Also, there was no significant difference between the use of either NaCl or $CaCl_2$ solution chemistry when applying DNAcol. Sticking efficiencies higher than 1 are physically impossible, since the fraction sticking to the sand grain surface cannot exceed the total fraction DNAcol colliding with the sand grain surface. We attributed this to the irregular shapes of the collector silica grains; the correlation equation we used in order to determine single collector efficiency was essentially developed for spherical collectors and not irregularly shaped collector grains, which likely gave rise to inaccuracies in determining sticking efficiencies. The calculated sticking efficiencies demonstrated that, in our experiments, a large fraction and in some experiments all DNAcol, colliding with the sand grain surface did also stick to the surface.

4. Discussion

In this work, we aimed at investigating the sensitivity of DNA-tagged silica particles to solution chemistry, and studied mechanisms controlling transport and retention. Based on the HYDRUS-1D modeling of the observed breakthrough curves we concluded, that the transport of DNAcol in columns of saturated quartz sand could be well described by a first order kinetic attachment and detachment rate coefficient. However, for several cases, we observed discrepancies between experimental data and the fitted model. Likely, more elaborate models including two kinetic sites, gravity effects, colloid-size dependent dispersivity, and/or nanoscale heterogeneity need to be invoked in order to further reduce these discrepancies, which we, however, considered to be outside the

Table 2
HYDRUS model parameters, statistics determined from curve fitting, and calculated sticking efficiencies.

	Q	[ml min^{-1}]	0.8	0.8	0.16	0.16
	d_g	[μm]	1000–1400	500–630	1000–1400	500–630
NaCl	λ_L	[cm]	2.8×10^{-2}	2.2×10^{-2}	1.6×10^{-2}	1.2×10^{-2}
	ε	[−]	0.45	0.43	0.4	0.44
DNA-DM	k_{att}	[min^{-1}]	9.37×10^{-03}	3.14×10^{-03}	2.68×10^{-04}	7.49×10^{-04}
	k_{det}	[min^{-1}]	1.07×10^{-01}	6.60×10^{-02}	2.32×10^{-03}	1.78×10^{-02}
	R^2	[%]	92	44	60	66
	α	[−]	2.72×10^{-01}	2.49×10^{-02}	8.45×10^{-03}	9.51×10^{-03}
DNA-NaCl	k_{att}	[min^{-1}]	5.88×10^{-04}	1.43×10^{-01}	4.91×10^{-02}	3.84×10^{-02}
	k_{det}	[min^{-1}]	6.89×10^{-02}	5.54×10^{-05}	3.08×10^{-05}	3.83×10^{-05}
	R^2	[%]	51	56	53	40
	α	[−]	1.71×10^{-02}	$1.13 \times 10^{+00}$	$1.55 \times 10^{+00}$	4.87×10^{-01}
DNA-$CaCl_2$	k_{att}	[min^{-1}]	5.78×10^{-03}	1.97×10^{-01}	3.55×10^{-02}	5.89×10^{-02}
	k_{det}	[min^{-1}]	5.25×10^{-02}	1.05×10^{-04}	8.56×10^{-06}	1.65×10^{-05}
	R^2	[%]	47	40	41	25
	α	[−]	1.68×10^{-01}	$1.56 \times 10^{+00}$	$1.12 \times 10^{+00}$	7.48×10^{-01}

scope of this work.

In their 14.5 cm sand columns, Saiers et al. (1994) arrived at a similar description of the silica colloid removal process, although their silica concentrations were much higher, the silica particles smaller (91 nm), and the zeta potential more negative (−65 mV). Furthermore, the ionic strength of the solutions they used was much lower (10^{-3} M NaCl and pH 8.5), while Darcian velocities (~5.7 cm hr^{-1}) were comparable to ours (2 and 10 cm hr^{-1}). The removal of silica in their case, however, was less than 10% (Fig. 1: Saiers et al., 1994), while in our case removal could be as high as 2–2.5 log-units or more than 90%. Johnson et al. (1996); their Fig. 2 used 10 cm columns of quartz sand (prolate spheroidal shaped, 0.32 nominal grain diameter), 300 nm silica colloids in dilute (10^{-3} M) KCl and, at comparable Darcian velocity or approach velocity as ours, arrived at similar first order kinetic removal of silica colloids, whereby their silica colloid removal rates (less than 5%) were in the same range as Saiers et al. (1994). We think this difference is due to a combination of higher ionic strength used (3.3×10^{-2} M NaCl and 4.1×10^{-2} M $CaCl_2$) in our work, larger DNAcol diameter, and a less negative zeta-potential of the DNAcol. Ionic strength matters, as is clear from the work of Zeng et al. (2017), Liu et al. (2017), and Wang et al. (2012). These authors used a first order kinetic removal mechanism, and observed a decrease in maximum relative concentration as a function of ionic strength of the solution. On the other hand, under high salinity conditions (8–10% *w/v* NaCl + $CaCl_2$ brines) Kim et al. (2015) observed aggregation of silica colloids, which could be transported through a 30 cm column of 0.35 mm Ottawa sand. The high Darcian flow (71 m day^{-1}) Kim et al. (2015) used, could well have contributed to the lack of first order kinetic attachment.

In addition to first order kinetic attachment, we used a first order kinetic rate constant to describe detachment of previously attached particles, while maintaining identical ionic strength conditions. In all cases, detachment during the tail of the breakthrough curve (from PV 4–6) did not lead to high $(C/C_0)_{DNAcol}$ values, and was a few orders of magnitude lower than maximum $(C/C_0)_{DNAcol}$ from PV 2–3. Detachment rate constants were generally higher for the DM water cases plus the fast flow-coarse sand experiments, while in most experiments using NaCl and $CaCl_2$ solutions, detachment rate constants were low (in the order of 10^{-4}–10^{-5}). Despite the use of a first order kinetic detachment rate constant, in literature, without exception, silica colloid breakthrough curves are shown using a linear vertical axis (Liu et al., 2017; Kim et al., 2015; Wang et al., 2012; Zeng et al., 2017; Saiers et al., 1994; Johnson et al., 1996; Vitorge et al., 2014, 2014a), emphasizing the effect of flow velocity on the normalized peak value concentration, and the type of plateau (e.g., steady-state, increasing or decreasing over time) but which does not make clear how (un)important the detachment process is.

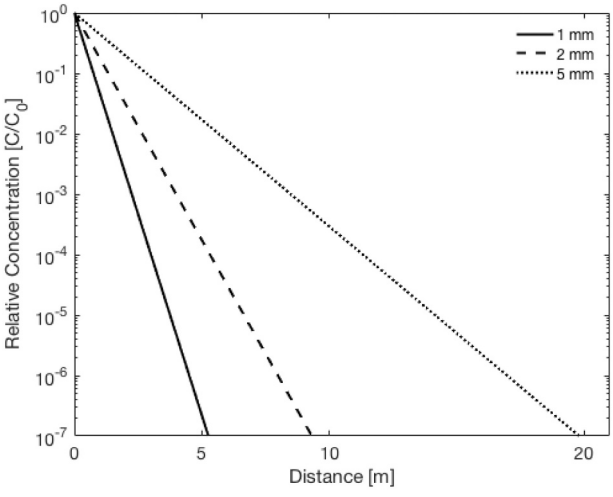

Fig. 2. Hypothetical case of DNAcol for various collector grain sizes (Darcy velocity = 300 m y^{-1}; sticking efficiency = 0.59; other parameter values: see a print-out of the calculation in the Supporting Information.

For the low flow NaCl and $CaCl_2$ cases (Fig. 1K, L, O, and P), at the end of the experiment, when we applied a flush of Milli-Q water, we observed massive reentrainment of previously attached particles. Zeng et al. (2017) also observed massive reentrainment of silica colloids due to DM water flushing at the end of their experiments, which was up to 800 times maximum C/C_0. They attributed this to strong electrostatic repulsion between sand collector and silica colloids as the surfaces of both materials possessed a high concentration of negative charge under the experimental conditions used (Zeng et al., 2017). Also, Liu et al. (2017), at the end of the column experiment after a flush of demineralised water, observed reentrainment of silica colloids up to 0.9 times maximum C/C_0. Their two-site dynamic model fitting results showed that reversible retention was related to first-order straining. Since the average diameter of the DNAcol in our case was 270 nm and the median of the finest grain size we used was ~565 μm, the ratio of the two was 4.8×10^{-4}, which was well below 0.003, defined by Bradford et al. (2007) to be the lowest ratio for spherical grains at which straining would occur. In other words, in our case, we think straining was relatively unimportant, and the observed reentrainment was due to electrostatic interaction variations as a result of the transient chemistry conditions we applied. In order to make our case, we calculated the DLVO profiles and added them to the Supporting Information. Since all zeta potential values were more negative than −20 mV, we assumed aggregation did not take place in our column experiments. From the DLVO profiles, a primary energy minimum and secondary energy minimum appeared for both NaCl and $CaCl_2$. However, in case of NaCl the energy barrier was higher (~600 K_BT) than for $CaCl_2$ (~100 K_BT), possibly giving rise to more attachment in the primary energy minimum for the latter case. Furthermore, the massive reentrainment of the attached DNAcol, when we applied the flushing step of Milli-Q water to the soil columns after NaCl and $CaCl_2$ experiments, was well explained by the DLVO profile in Milli-Q water.

From calculating the sticking efficiencies, we concluded that a large fraction, if not all, DNAcol colliding with the sand grain surface did also stick to that sand grain surface. From the reentrainment of DNAcol under transient chemistry conditions, we also conclude that in terms of DLVO theory, a large fraction of retained DNAcol resided in the secondary energy minimum. Hereby we assumed a negative charge for both silica sand and DNAcol, giving rise to a primary energy minimum due to attractive Van der Waals forces at close distance of the sand grain (nm range), an energy barrier further away, followed by a secondary energy minimum as a result of the net electrostatic forces between DNAcol and sand grain. In literature, we have not come across sticking efficiency values for silica colloid – silica collector grains under conditions of similarly charged surfaces. From transport of bacteria and viruses in aquifers, we know that sticking efficiencies must be in the order of 10^{-4} for viruses and 10^{-3} for bacteria in order to be able to travel through an aquifer (e.g. Foppen and Schijven, 2006), as sticking efficiencies in the order of 0.1–1 lead to the immediate removal of the biocolloid at short distance from where it enters the aquifer. Assuming a sticking efficiency of 0.59, which is the average of all our experiments, and a Darcy flow velocity of 300 m y^{-1}, and a porosity of 0.35, we determined the relative DNAcol concentration as a function of transport distance (Fig. 2) upon traveling through aquifers composed of 1–5 mm size silica grains. If the vial of 1 ml 10 mg ml^{-1} DNAcol suspension we used in this study, equal to $\sim 4 \times 10^{11}$ particles ml^{-1}, would have been completely diluted in 1 l aquifer water, which would have been injected into the aquifer without further dilution, and if we assume a lowest limit of detection of 5 individual DNAcol in a 4 μl sample in a qPCR well (or 1.25×10^5 DNAcol per l), then a removal of $4 \times 10^{11}/1.25 \times 10^5 = 3.2 \times 10^6$ can be allowed for detection. This assumes no further dilution will take place due to diverging or converging flow lines in the aquifer (e.g. due to injection or abstraction). Also, this assumes the aquifer is fully composed of negative surface charge, which is, due to the presence of minerals like calcite or

iron (III) oxyhydroxide coatings around aquifer grains, not very realistic. In such cases, removal of DNAcol will likely be higher (Li and Cathles, 2014; Johnson et al., 1996; Ryan et al., 1999). Finally, this assumes no detachment is taking place, which is not true: in reality detachment takes place, but with such slow detachment rate that it has negligible effect.

For an aquifer composed of 1 mm silica grains, the maximum traveled distance would be ~5 m and for a 5 mm silica grain aquifer, maximum travel distance would be ~20 m. Larger transport distances are of course possible by increasing DNAcol injection mass or by up-concentrating sample volumes. This example serves to illustrate the potential of DNAcol: for fine grained aquifers (e.g. silts, clays, or mixtures) DNAcol will have limited applicability under natural groundwater chemistry, since the particle will not travel very far. Straining of DNAcol in such conditions will of course further limit DNAcol transport. Also, due to this DNAcol mass loss (attachment, straining, etc.), it will be impossible to determine the entire DNAcol mass and to prepare a mass balance. Also, since chemical conditions in the aquifer will be transient in nature by default, previously attached DNAcol can likely be reentrained. For aquifers predominantly composed of silica, DNAcol can be used in high concentrations in case of short distance, high flow, coarse aquifer grain conditions to map contaminant sources, understand flowpaths and determine travel times. There is a fair chance the aquifer grains will be covered by a layer of humic substances and/or a biofilm. In those cases, reaching the secondary minimum might be sterically hindered, which reduces DNAcol attachment and increases transport distance. On the other hand, Zhang et al. (2020) observed clustering of Si nanoparticles and humic acid due to calcium bridging, which increased retention, due to the presence of Ca^{2+}, so those same humic substances can also increase attachment and reduce transport distance. Finally, the DNAcol can be pre-conditioned, whereby the formation of an eco-corona at the outer surface of each individual DNA silica colloid is allowed to take place (e.g. Xu et al., 2020; Galloway et al., 2017; Lynch et al., 2014), in order to reduce removal and to enhance DNAcol transport. For those conditions, the fate of each unique DNAcol should be studied, and more research work is required.

5. Conclusions

We are the first to explore the deposition kinetics of this new DNA-tagged silica tracer for different pore water chemistries, flow rates, and sand grain size distributions in a series of saturated sand column experiments in order to predict environmental conditions for which the DNA-tagged silica tracer can best be employed.

Based on the HYDRUS modeling of the observed breakthrough curves, we concluded that the transport of the DNAcol in columns of saturated quartz sand could be well described by a first order kinetic attachment and detachment rate coefficient. Attachment was primarily in the secondary energy minimum, so the DNAcol could be reentrained under transient flow conditions.

Based on calculated average sticking efficiencies, we concluded that a large fraction, if not all, the DNAcol colliding with the sand grain surface did also stick to that sand grain surface. Therefore, the potential of current DNAcol as a tracer for fine grained aquifers (e.g. fine sand, silts and natural groundwater) will be limited, since the particle will not travel very far. For such cases, DNAcol with different physio-chemical characteristics need to be developed. For sandy aquifers, the DNAcol can be used potentially in high concentrations in case of short distance (i.e. meter scale), high flow velocities, coarse aquifer grain conditions and distinct preferential flow paths to map contaminant sources, understand flowpaths and determine travel times.

Overall, the DNAcol exhibited some limitations for the application as a generic hydrological tracer in subsurface flow, especially in the presence of fine grains or low flow velocity. Despite such limitations, DNAcol showed potential to be used as colloidal tracer to study fate and transport of biological and engineered colloidal particles (like pathogens or microplastics).

Declaration of Competing Interest

The authors declare that they have no known competing financial interests or personal relationships that could have appeared to influence the work reported in this paper.

Acknowledgment

This research is supported financially by Netherlands Organization for Scientific Research (NWO), TTW grant 14514 WaterTagging. We are grateful to Prof. Robert N. Grass, Dr. Gediminas Mekutis, and Dr. Julian Koch (Department of Chemistry and Applied Biosciences ETH Zurich), for providing us DNA particle tracers. We thank Yvonne Hoiting, and Ali Ben Hadi for their laboratory support of qPCR analyses, and Jesse van der Hoeven (Utrecht University, the Netherlands) for his contribution during early stage of this research. We thank IHE-Delft for the laboratory access and support. We would like to thank the anonymous reviewers for their constructive feedbacks on this manuscript.

Appendix A. Supplementary data

Supplementary data to this article can be found online at https://doi.org/10.1016/j.jconhyd.2022.103954.

References

Bedrikovetsky, P., Siqueira, F.D., Furtado, C., de Souza, A.L.S., 2011. Modified particle detachment model for colloidal transport in porous media. J. Transp. Porous Media 86, 353–383.

Bedrikovetsky, P., Zeinijahromi, A., Siqueira, F.D., Furtado, C., de Souza, A.L.S., 2012. Particle detachment under velocity alternation during suspension transport in porous media. J. Transp. Porous Media 91 (1), 173–197.

Bradford, S., Torkzaban, S., Walker, S.L., 2007. Coupling physical and chemical mechanisms of colloid straining in saturated porous media. Water Res. 41, 3012–3024.

Bradford, S.A., Kim, H., Haznedaroglu, B.Z., Torkzaban, S., Walker, S.L., 2009. Coupled factors influencing concentration-dependent colloid transport and retention in saturated porous media. Environ. Sci. Technol. 43, 6996–7002.

Bradford, S.A., Torkzaban, S., Leij, F., Simunek, J., 2015. Equilibrium and kinetic models for colloid release under transient solution chemistry conditions. J. Contam. Hydrol. 181 (2015), 141–152.

Chrysikopoulos, C.V., Katzourakis, V.E., 2015. Colloid particle size-dependent dispersivity. Water Resour. Res. 51 (6), 4668–4683. https://doi.org/10.1002/2014WR016094.

Chrysikopoulos, C.V., Syngouna, V.I., 2014. Effect of gravity on colloid transport through water-saturated columns packed with glass beads: modeling and experiments. Environ. Sci. Technol. 48 (12), 6805–6813. https://doi.org/10.1021/es501295n.

Dai, C., Zhou, H., You, X., Duan, Y., Tu, Y., Liu, S., Zhou, F., Hon, L.K., 2020. Silica colloids as non-carriers facilitate Pb2+ transport in saturated porous media under a weak adsorption condition: effects of Pb2+ concentrations. Environ. Sci. Pollut. Res. 27 (13), 15188–15197. https://doi.org/10.1007/s11356-020-08064-0.

de Oliveira, E.M., Garcia-Rojas, E.E., Valadão, I.C.R.P., Araújo, A.S.F., de Castro, J.A., 2017. Effects of the silica nanoparticles (NPSiO2) on the stabilization and transport of hazardous nanoparticle suspensions into landfill soil columns. Revista Escola de Minas 70 (3), 317–323. https://doi.org/10.1590/0370-44672015700204.

Elimelech, M., Gregory, J., Jia, X., Williams, R.A., 1995. Particle Deposition and Aggregation. Measurement, Modelling and Simulation. Published at Butterworth-Heinemann. ISBN 0-7506-7024-X.

Foppen, J.W.A., Schijven, J.F., 2006. Transport and survival of *Escherichia coli* and thermotolerant coliforms in aquifers under saturated conditions – a review. Water Res. 40, 401–426.

Foppen, J.W., Seopa, J., Bakobie, N., Bogaard, T., 2013. Development of a methodology for the application of synthetic DNA in stream tracer injection experiments. Water Resour. Res. 49 (9), 5369–5380. https://doi.org/10.1002/wrcr.20438.

Galloway, T., Cole, M., Lewis, C., 2017. Interactions of microplastic debris throughout the marine ecosystem. Nat. Ecol. Evol. 1, 0116. https://doi.org/10.1038/s41559-017-0116.

Grass, R.N., Schälchli, J., Paunescu, D., Soellner, J.O.B., Kaegi, R., Stark, W.J., 2014. Tracking trace amounts of submicrometer silica particles in wastewaters and activated sludge using silica-encapsulated DNA barcodes. Environ. Sci. Technol. Lett. 1 (12), 484–489. https://doi.org/10.1021/ez5003506.

Harvey, R.W., Garabedian, S.P., 1991. Use of colloid filtration theory in modeling movement of bacteria through a contaminated sandy aquifer. Environ. Sci. Technol. 25, 178–185.

Higgo, J.J.W., Williams, G.M., Harrison, I., Warwick, P., Gardiner, M.P., Longworth, G., 1993. Colloid transport in a glacial sand aquifer. Laboratory and field studies. Colloids Surf. A Physicochem. Eng. Asp. 73 (C), 179–200. https://doi.org/10.1016/0927-7757(93)80015-7.

Hou, W., Lei, Z., Hu, E., Wang, H., Wang, Q., Zhang, R., Li, H., 2021. Co-transport of uranyl carbonate and silica colloids in saturated quartz sand under different hydrochemical conditions. Sci. Total Environ. https://doi.org/10.1016/j.scitotenv.2020.142716 art. no. 142716.

Johnson, P.R., Sun, N., Elimelech, M., 1996. Colloid transport in geochemically heterogeneous porous media: modelling and measurements. Environ. Sci. Technol. 1996 (30), 3284–3293.

Katzourakis, V.E., Chrysikopoulos, C.V., 2017. Fitting the transport and attachment of dense biocolloids in one-dimensional porous media: ColloidFit. Groundwater 55 (2), 156–159. https://doi.org/10.1111/gwat.12501.

Katzourakis, V.E., Chrysikopoulos, C.V., 2019. Two-site colloid transport with reversible and irreversible attachment: analytical solutions. Adv. Water Resour. 130, 29–36. https://doi.org/10.1016/j.advwatres.2019.05.026.

Kim, I., Taghavy, A., DiCarlo, D., Huh, C., 2015. Aggregation of silica nanoparticles and its impact on particle mobility under high-salinity conditions. J. Pet. Sci. Eng. 133, 376–383. https://doi.org/10.1016/j.petrol.2015.06.019.

Kittilä, A., Jalali, M.R., Evans, K.F., Willmann, M., Saar, M.O., Kong, X.-Z., 2019. Field comparison of DNA-labeled nanoparticle and solute tracer transport in a fractured crystalline rock. Water Resour. Res. 55 (8), 6577–6595. https://doi.org/10.1029/2019WR025021.

Ko, C.-H., Chen, J.Y., 2000. Dynamics of silica colloid deposition and release in packed beds of aminosilane-modified glass beads. Langmuir 16 (17), 6906–6912. https://doi.org/10.1021/la000415y.

Koch, J., Gantenbein, S., Masania, K., Stark, W.J., Erlich, Y., Grass, R.N., 2020. A DNA-of-things storage architecture to create materials with embedded memory. Nat. Biotechnol. 38 (1), 39–43. https://doi.org/10.1038/s41587-019-0356-z.

Kong, X.-Z., Deuber, C.A., Kittilä, A., Somogyvári, M., Mikutis, G., Bayer, P., Stark, W.J., Saar, M.O., 2018. Tomographic reservoir imaging with DNA-labeled silica Nanotracers: the first field validation. Environ. Sci. Technol. 52 (23), 13681–13689. https://doi.org/10.1021/acs.est.8b04367.

Li, Y.V., Cathles, L.M., 2014. Retention of silica nanoparticles on calcium carbonate sands immersed in electrolyte solutions. J. Colloid Interface Sci. 436, 1–8. https://doi.org/10.1016/j.jcis.2014.08.072.

Liu, C., Xu, N., Feng, G., Zhou, D., Cheng, X., Li, Z., 2017. Hydrochars and phosphate enhancing the transport of nanoparticle silica in saturated sands. Chemosphere 189, 213–223. https://doi.org/10.1016/j.chemosphere.2017.09.066.

Liu, Q., Sun, Z., Santamarina, J.C., 2019. Transport and adsorption of silica nanoparticles in carbonate reservoirs: a sand column study. Energy Fuel 33 (5), 4009–4016. https://doi.org/10.1021/acs.energyfuels.9b00057.

Long, W., Hilpert, M., 2009. A correlation for the collector efficiency of Brownian particles in clean-bed filtration in sphere packings by a lattice-Boltzmann method. Environ. Sci. Technol. 43 (12), 4419–4424.

Lutterodt, G., Foppen, J.W.A., Uhlenbrook, S., 2021. Transport of *Escherichia coli* strains isolated from natural spring water. J. Contam. Hydrol. 140–141, 12–20. https://doi.org/10.1016/j.jconhyd.2012.08.011.

Lynch, I., Dawson, K.A., Lead, J.R., Valsami-Jones, E., 2014. Macromolecular coronas and their importance in Nanotoxicology and Nanoecotoxicology. Front. Nanosci. 7, 127–156. https://doi.org/10.1016/B978-0-08-099408-6.00004-9.

Ma, H., Hradisky, M., Johnson, W.P., 2013. Extending applicability of correlation equations to predict colloidal retention in porous media at low fluid velocity. Environ. Sci. Technol. 47 (5), 2272–2278.

Marquardt, D.W., 1963. An algorithm for least-squares estimation of nonlinear parameters. SIAM J. Appl. Math. 11 (431–441), 1963.

Mikutis, G., Deuber, C.A., Schmid, L., Kittilä, A., Lobsiger, N., Puddu, M., Asgeirsson, D. O., Grass, R.N., Saar, M.O., Stark, W.J., 2018. Silica-encapsulated DNA-based tracers for aquifer characterization. Environ. Sci. Technol. 52 (21), 12142–12152. https://doi.org/10.1021/acs.est.8b03285.

Molnar, I.L., Johnson, W.P., Gerhard, J.I., Willson, C.S., O'Carroll, D.M., 2015. Predicting colloid transport through saturated porous media: a critical review. Water Resour. Res. 51 (9), 6804–6845. https://doi.org/10.1002/2015WR017318.

Molnar, I.L., Pensini, E., Asad, M.A., Mitchell, C.A., Nitsche, L.C., Pyrak-Nolte, L.J., Miño, G.L., Krol, M.M., 2019. Colloid transport in porous media: a review of classical mechanisms and emerging topics. Transp. Porous Media 130 (1), 129–156. https://doi.org/10.1007/s11242-019-01270-6.

Mora, C.A., Paunescu, D., Grass, R.N., Stark, W.J., 2015. Silica particles with encapsulated DNA as trophic tracers. Mol. Ecol. Resour. 15 (2), 231–241. https://doi.org/10.1111/1755-0998.12299.

Nelson, K.E., Ginn, T.R., 2011. New collector efficiency equation for colloid filtration in both natural and engineered flow conditions. Water Resour. Res. 47, W05543. https://doi.org/10.1029/2010WR009587.

Paunescu, D., Puddu, M., Soellner, J.O.B., Stoessel, P.R., Grass, R.N., 2013. Reversible DNA encapsulation in silica to produce ROS-resistant and heat-resistant synthetic DNA 'fossils'. Nat. Protoc. 8 (12), 2440–2448. https://doi.org/10.1038/nprot.2013.154.

Qin, Y., Wen, Z., Zhang, W., Chai, J., Liu, D., Wu, S., 2020. Different roles of silica nanoparticles played in virus transport in saturated and unsaturated porous media. Environ. Pollut. 259 https://doi.org/10.1016/j.envpol.2019.113861 art. no. 113861.

Rajagopalan, R., Tien, C., 1976. Trajectory analysis of deep-bed filtration with sphere-in-cell porous-media model. AICHE J. 22 (3), 523–533.

Rhodes, M.J., 2008. Introduction to Particle Technology. John Wiley & Sons.

Ron, C.A., Johnson, W.P., 2020. Complementary colloid and collector nanoscale heterogeneity explains microparticle retention under unfavorable conditions. Environ. Sci. Nano 7 (12), 4010–4021. https://doi.org/10.1039/d0en00815j.

Ron, C.A., Vanness, K., Rasmuson, A., Johnson, W.P., 2019. How nanoscale surface heterogeneity impacts transport of nano- to micro-particles on surfaces under unfavorable attachment conditions. Environ. Sci. Nano 6 (6), 1921–1931. https://doi.org/10.1039/c9en00306a.

Ryan, J.N., Elimelech, M., 1996. Colloid mobilization and transport in groundwater. Colloids Surf. A Physicochem. Eng. Asp. 107, 1–56. https://doi.org/10.1016/0927-7757(95)03384-X.

Ryan, J.N., Elimelech, M., Ard, R.A., Harvey, R.W., Johnson, P.R., 1999. Bacteriophage PRD1 and silica colloid transport and recovery in an iron oxide-coated sand aquifer. Environ. Sci. Technol. 33 (1), 63–73. https://doi.org/10.1021/es980350+.

Saiers, J.E., Hornberger, G.M., Harvey, C., 1994. Colloidal silica transport through structured, heterogeneous porous media. J. Hydrol. 163 (3–4), 271–288. https://doi.org/10.1016/0022-1694(94)90144-9.

Schijven, J.F., Šimůnek, J., 2002. Kinetic modeling of virus transport at the field scale. J. Contam. Hydrol. 55 (1–2), 113–135. https://doi.org/10.1016/S0169-7722(01)00188-7.

Scotoni, M., Koch, J., Julian, T.R., Clack, L., Pitol, A.K., Wolfensberger, A., Grass, R.N., Sax, H., 2020. Silica nanoparticles with encapsulated DNA (SPED) - a novel surrogate tracer for microbial transmission in healthcare. Antimicrob. Resist. Infect. Control 9 (1). https://doi.org/10.1186/s13756-020-00813-7 art. no. 152.

Selim, H.M., Schulin, R., Fluehler, H., 1987. Transport and ion exchange of calcium and magnesium in an aggregated soil. Soil Sci. Soc. Am. J. 51 (4), 876–884. https://doi.org/10.2136/sssaj1987.03615995005100040007x.

Šimůnek, J., van Genuchten, M.Th., 2008. Modeling nonequilibrium flow and transport processes using HYDRUS. Vadose Zone J. 7, 782–797. https://doi.org/10.2136/vzj2007.0074.

Šimůnek, J., van Genuchten, M.Th., Gribb, M.M., Hopmans, J.W., 1998. Parameter Estimation of Unsaturated Soil Hydraulic Properties from Transient Flow Processes, Soil & Tillage Research, 47/1–2, Special Issue "State of the Art in Soil Physics and in Soil Technology of Antrophic Soils", pp. 27–36.

Šimůnek, J., Šejna, M., Saito, H., Sakai, M., van Genuchten, M.Th., 2013. The HYDRUS-1D Software Package for Simulating the One-Dimensional Movement of Water, Heat, and Multiple Solutes in Variably-Saturated Media. From. https://www.pc-progress.com/Downloads/Pgm_hydrus1D/HYDRUS1D-4.17.pdf.

Tufenkji, N., Elimelech, M., 2004. Correlation equation for predicting single-collector efficiency in physicochemical filtration in saturated porous media. Environ. Sci. Technol. 38 (2), 529–536.

Van Genuchten, M., 1981. Analytical solutions for chemical transport with simultaneous adsorption, zero-order production and first-order decay. J. Hydrol. 49, 213–233.

Van Genuchten, M.T., Wagenet, R.J., 1989. Two-site/two-region models for pesticide transport and degradation: theoretical development and analytical solutions. Soil Sci. Soc. Am. J. 53 (5), 1303–1310. https://doi.org/10.2136/sssaj1989.03615995005300050001x.

Van Genuchten, M.Th., Šimůnek, J., Leij, F.J., Toride, N., Šejna, M., 2012. Stanmod: model use, calibration, and validation. Trans. ASABE 55 (4), 1353–1366.

Vitorge, E., Szenknect, S., Martins, J.M.F., Barthès, V., Auger, A., Renard, O., Gaudet, J.-P., 2014. Comparison of three labeled silica nanoparticles used as tracers in transport experiments in porous media. Part I: syntheses and characterizations. Environ. Pollut. 184, 605–612. https://doi.org/10.1016/j.envpol.2013.07.031.

Vitorge, E., Szenknect, S., Martins, J.M.-F., Barthès, V., Gaudet, J.-P., 2014a. Comparison of three labeled silica nanoparticles used as tracers in transport experiments in porous media. Part II: transport experiments and modeling. Environ. Pollut. 184, 613–619. https://doi.org/10.1016/j.envpol.2013.08.016.

Wang, C., Bobba, A.D., Attinti, R., Shen, C., Lazouskaya, V., Wang, L.-P., Jin, Y., 2012. Retention and transport of silica nanoparticles in saturated porous media: effect of concentration and particle size. Environ. Sci. Technol. 46 (13), 7151–7158. https://doi.org/10.1021/es300314n.

Xu, L., Xu, M., Wang, R., Yin, Y., Lynch, I., Liu, S., 2020. The crucial role of environmental coronas in determining the biological effects of engineered nanomaterials. Small 16 (36). https://doi.org/10.1002/smll.202003691 art. no. 2003691.

Yao, K.-M., Habibian, M.T., O'Melia, C.R., 1971. Water and waste water filtration. Concepts and applications. Environ. Sci. Technol. 5 (11), 1105–1112.

Zeng, C., Shadman, F., Sierra-Alvarez, R., 2017. Transport and abatement of fluorescent silica nanoparticle (SiO2 NP) in granular filtration: effect of porous media and ionic strength. J. Nanopart. Res. 19 (3) https://doi.org/10.1007/s11051-017-3808-8 art. no. 105.

Zhang, Y., Manley, T.S., Li, K., Horne, R.N., 2015. DNA-Encapsulated Silica Nanoparticle Tracers for Fracture Characterization. From. https://www.researchgate.net/publication/348579696_DNA-Encapsulated_Silica_Nanoparticle_Tracers_for_Fracture_Characterization.

Zhang, M., Li, D., Ye, Z., Wang, S., Xu, N., Wang, F., Liu, S., Chen, J., Gu, H., 2020. Effect of humic acid on the sedimentation and transport of nanoparticles silica in water-saturated porous media. J. Soils Sediments 20 (2), 911–920. https://doi.org/10.1007/s11368-019-02444-x.

Zhou, J., Zhang, W., Liu, D., Wang, Z., Li, S., 2017. Influence of humic acid on the transport and deposition of colloidal silica under different hydrogeochemical conditions. Water (Switzerland) 9 (1). https://doi.org/10.3390/w9010010 art. no. 10.